Volume 4
Number 23
7 December 2023
Pages 5853–6452

Materials Advances

rsc.li/materials-advances

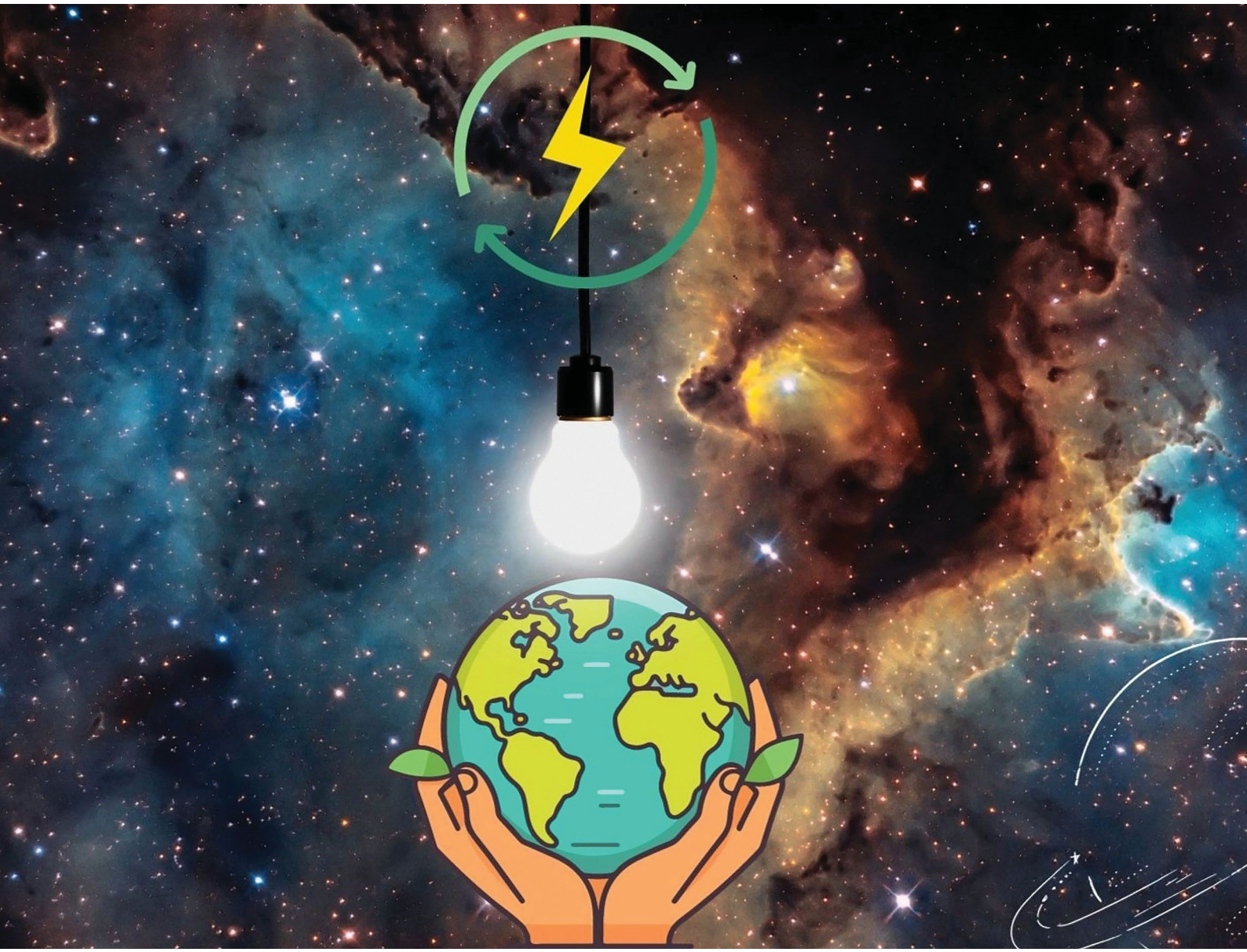

ISSN 2633-5409

ROYAL SOCIETY OF CHEMISTRY

PAPER
Ashok M. Sajjan *et al.*
The state of understanding of the electrochemical behaviours of a valve-regulated lead–acid battery comprising manganese dioxide-impregnated gel polymer electrolyte

Materials Advances

ROYAL SOCIETY OF CHEMISTRY

PAPER

View Article Online
View Journal | View Issue

Cite this: *Mater. Adv.*, 2023, 4, 6192

The state of understanding of the electrochemical behaviours of a valve-regulated lead–acid battery comprising manganese dioxide-impregnated gel polymer electrolyte

Bipin S. Chikkatti,[a] Ashok M. Sajjan *[ab] and Nagaraj R. Banapurmath [b]

Received 18th August 2023,
Accepted 29th September 2023

DOI: 10.1039/d3ma00563a

rsc.li/materials-advances

Gel electrolyte plays a vital role in the valve-regulated lead acid battery. To address this, we formulate a gel polymer electrolyte containing poly(vinyl alcohol) as the base matrix and manganese dioxide as an additive. The addition of manganese dioxide into poly(vinyl alcohol) increases the ionic conductivity of the gel. Chemical interaction between poly(vinyl alcohol) and manganese dioxide is confirmed by Fourier transform infrared spectroscopy. Electrochemical characterisations such as cyclic voltammetry, electrochemical impedance spectroscopy and potentiodynamic polarisation suggest that 3 wt% manganese dioxide in the poly(vinyl alcohol) gel system displays better electrochemical performance. The galvanostatic charge–discharge technique reveals that the battery device with an optimised gel system showed the highest discharge capacity of 9.080 μA h at a current density of 87.5 μA cm^{-2} and 81% discharge capacity after 500 steady cycles.

Introduction

In previous decades, new research initiatives focused on the creation of enhanced lead–acid batteries with increased power, durability, and dependability given by the use of innovative materials now being developed.[1] The most popular kind of rechargeable battery is still the lead–acid battery, which is used in many different things including telecommunications, solar traffic lights, uninterruptible power sources, stationary and traction applications, and automobiles. Although inexpensive, lead–acid batteries have a low energy density when compared to other innovative energy storage methods. Fast charging may be able to address the disadvantage of lead–acid batteries in particular applications, such as utility vehicles and forklift trucks. Utility cars with quick battery recharge during brief pauses perform almost as well as those with more sophisticated batteries.[2] The management of the oxygen cycle, the design of grid alloy and separators, and the optimisation of the charge methods have all required significant technological effort in the evolution of the valve-regulated lead–acid (VRLA) battery from its flooded parent during the last few years.[3] Due to its inherent qualities of being low maintenance, simple to install, even in the rack of commuting equipment, having no gas release, producing a clean product, and being affordable, VRLA batteries are the favoured option for energy storage.[4]

In the construction of VRLA batteries, gelling the sulphuric acid solution and subsequently immobilising the electrolyte are crucial phases.[5] Gel polymeric electrolytes are often swollen polymer networks, so they possess both the cohesive properties of solids and the properties of the liquids from the point of view of diffusive transport.[6] In recent years, several polymers like poly(methyl methacrylate),[7] polyacrylamide,[8] calcium alginate,[9] poly(acrylonitrile) (PAN)[10] and poly(vinyl alcohol)[11] have been used for the preparation of gel electrolytes. When poly(vinyl acetate) is subjected to alcoholysis, hydrolysis, or ammonolysis, a long-chain water-soluble polymer known as poly(vinyl alcohol) (PVA) is produced. PVA-based hydrogels are a colloidal dispersion with swelling and crosslinking creating three-dimensional network architectures.[12] Because of its low toxicity, accessibility, affordability, and environmental friendliness, PVA-based gel electrolytes have received a lot of research attention.[13] The generation of polymer electrolytes is caused by –OH groups in the host matrix PVA that are linked to the methane carbon of the backbone carbon chain.[14] The performance of energy storage devices is severely constrained by their typical weak water retention ability, quick fatigue under substantial deformation, and poor conductivity.[15] Demerits of PVA can be overcome by adding plasticizers like metal oxides, conductive polymers, nanomaterials, *etc.* Wang *et al.* reported that PVA can be used for the preparation of multifunctional gel electrolyte composites.[16]

[a] *Department of Chemistry, KLE Technological University, Hubballi 580031, India. E-mail: am_sajjan@kletech.ac.in*
[b] *Centre of Excellence in Material Science, School of Mechanical Engineering, KLE Technological University, Hubballi 580031, India*

Conductive metal oxides have a band gap of 0 eV or less, which means that electrons can easily move from the valence band to the conduction band. This allows for the free flow of electrons, which makes the material conductive.[17] Some examples of conductive metal oxides include ZnO, SnO_2, NiO, Cu_2O, In_2O_3 and MnO_2. Manganese dioxide (MnO_2) is generally recognized as one of the most promising candidates because of its large theoretical capacity and high working voltage.[18] MnO_2 is a good conductor of electricity because it has a partially filled 3d electron shell. This means that there are electrons that are free to move around, which allows for the flow of electricity.[19] The conductivity of MnO_2 is due to a combination of factors, including the partially filled 3d electron shell, the crystal structure, and temperature. This makes MnO_2 a useful material for a variety of applications, including batteries,[20] sensors,[21] supercapacitors[22] and catalysts.[23] Li *et al.* in 2012 reported that MnO_2 can be used as a conductive material to increase the electrochemical performance of energy storage devices.[24]

To realize the practical applications of MnO_2 in lead acid batteries, we formulated a PVA-based gel electrolyte comprising MnO_2 as an additive. We used the Fourier transform infrared spectroscopy (FTIR) technique to understand the interaction between PVA and MnO_2. The gel systems were subjected to electrochemical tests like cyclic voltammetry (CV), electrochemical impedance spectroscopy (EIS), potentiodynamic polarisation (PDP) and galvanostatic charge–discharge (GCD) tests to analyse their electrochemical behaviour. An increase in ionic conductivity after the addition of MnO_2 into PVA gel evidenced that the MnO_2@PVA gel system can be used to enhance the electrochemical performance of the VRLA battery.

Experimental

Chemicals

Poly(vinyl alcohol) (M_w ~ 124 000) was purchased from S. D. Fine Chemicals Ltd, Mumbai, India. Manganese dioxide (M_w ~ 86.94) was provided by Reachem Laboratory Chemicals Private Limited, Chennai, India. Sulphuric acid was provided by Spectrum Reagent and Chemicals Pvt. Ltd, Cochin, India. Demineralized water was used throughout the experiment.

Formulation of gel systems

PVA gel electrolyte was prepared by dissolving 4 wt% of PVA in 36 wt% of H_2SO_4 by heating at 60 °C with continuous stirring until a homogenous viscous solution was formed. The obtained gel electrolyte is called plane PVA. In order to prepare MnO_2-incorporated PVA gel electrolytes, a known amount of MnO_2 is added to the PVA gel electrolyte and the solution was stirred for 24 hours at room temperature. However, the amount of MnO_2 concerning PVA was varied as 1, 3, 5, and 7 wt% and the resultant gel electrolytes were designated as 1 wt% MnO_2@PVA, 3 wt% MnO_2@PVA, 5 wt% MnO_2@PVA and 7 wt% MnO_2@PVA respectively. Fig. 1(a) represents the hydrogen-bonded interaction between MnO_2 and PVA. Fig. 1(b) displays photo images of the synthesized gel systems.

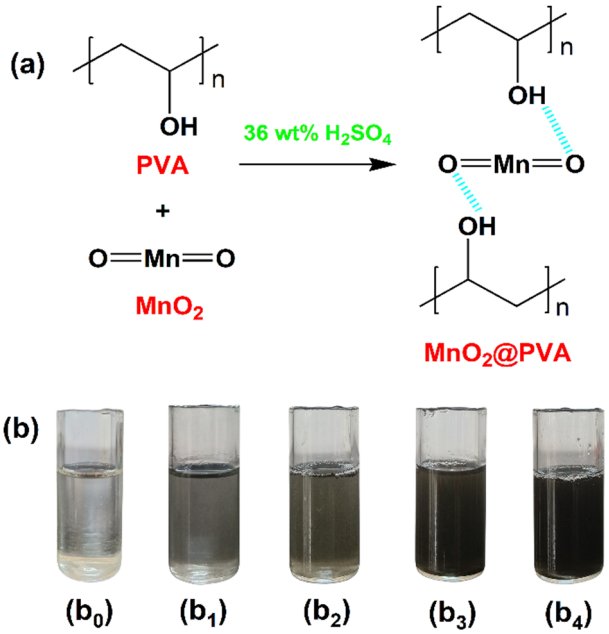

Fig. 1 (a) Interaction between MnO_2 and PVA. (b) Photo images of (b_0) plane PVA, (b_1) 1 wt% MnO_2@PVA, (b_2) 3 wt% MnO_2@PVA, (b_3) 5 wt% MnO_2@PVA and (b_4) 7 wt% MnO_2@PVA gel electrolytes.

Characteristic study of the gel systems

To establish the interaction between MnO_2 and PVA in the gel structure, the gels were submitted to FTIR analysis (PerkinElmer Pvt. Ltd, Singapore). The conductivity meter type EQ-662 (Equip-Tronics, Mumbai, India) was used to measure the ionic conductivity of the gels. Techniques such as CV, EIS, PDP, and GCD were used to examine the electrochemical nature of the gel formulations. When recording the CV curves, several scan rates between 10 and 100 mV s^{-1} were used while maintaining a potential range of −1 to +1 V. At each OCP, EIS measurements were conducted at frequencies ranging from 1 Hz to 100 kHz with amplitudes of 5 mV. By understanding the various OCPs, PDP tests were performed at a scan rate of 10 mV s^{-1}. We designed a prototype battery with an improved gel electrolyte, and to evaluate how it operated, GCD tests at various current densities were conducted, along with a cycle analysis. In the electrochemical analyser (CHI660E, CH Instruments, Texas, USA), we employed a three-electrode system for CV, EIS, and PDP and a two-electrode system for GCD. A lead electrode, platinum wire and Ag/AgCl, (saturated) KCl are the working electrode, counter electrode and reference electrode, respectively. Before analysis, the lead electrode was polished, taking care to avoid touching the electrodes. All experiments were conducted at a 25 °C temperature.

Results and discussion

FTIR analysis

The FTIR spectrum of MnO_2 powder is presented in Fig. 2(a). O–H stretching vibrations are attributed to the broadband of about 3446 cm^{-1}, showing that MnO_2 is a hydrate.[25] The bending

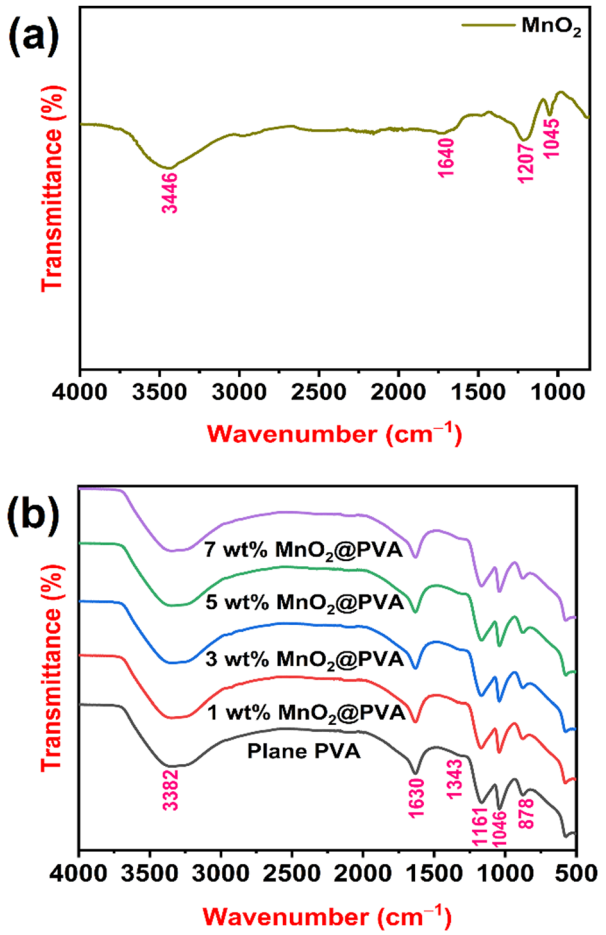

Fig. 2 FTIR spectra of (a) MnO_2 powder, and (b) plane PVA and PVA loaded with different wt% of MnO_2.

vibrations of the O–H groups from water molecules that were absorbed were likely the cause of the weak band at 1640 cm^{-1}.[26] O–H coupled with Mn atoms is considered to be the source of the bending vibrations in the absorption bands at about 1207 cm^{-1} and 1045 cm^{-1}.[27] Fig. 2(b) displays the FTIR spectra of plane PVA and PVA loaded with different wt% of MnO_2. The main peaks of PVA were observed at 3382, 1630, 1161 and 1046 cm^{-1}. The peak at 3382 cm^{-1} is assigned to the O–H stretching vibration of the hydroxy group. The C=O carbonyl stretch causes the peak at 1630 cm^{-1}.[28] The two peaks at 1161 cm^{-1} and 1046 cm^{-1} correspond to C–O stretching of acetyl groups.[29] As the content of MnO_2 increases in the PVA matrix, the expansion of these characteristic peaks marginally decreases, indicating the influence of the MnO_2 content in the polymer matrix. This also indicates that the MnO_2 particles are intercalating between the PVA chains, which restricts the mobility of the polymer chains and reduces the interlayer spacing.[30] Furthermore, the peaks at 1343 cm^{-1} and 878 cm^{-1} are associated with the stretching vibrations of S=O and S–OH in H_2SO_4 in the gel systems.[31,32]

Ionic conductivity study

Ionic conductivity is electrical conductivity due to the motion of ionic charge.[33] Fig. 3(a) displays the ionic conductivity findings of all gel systems. The ionic conductivity of plane PVA or 0 wt% MnO_2@PVA was 7.6 mS cm^{-1}. The ionic conductivity values of the MnO_2@PVA gel systems were higher than those of plane PVA. The ionic conductivities of 1 wt% MnO_2@PVA, 3 wt% MnO_2@PVA, 5 wt% MnO_2@PVA and 7 wt% MnO_2@PVA gel electrolytes were 7.63, 7.85, 7.79 and 7.76 mS cm^{-1}, respectively. As the content of MnO_2 in the PVA gel system increases from 1 wt% to 3 wt%, ionic conductivity also increases. This is because the MnO_2 particles interact with the polymer chains, creating a more open and flexible network. This allows the ions to move more easily through the electrolyte, resulting in higher ionic conductivity.[34] Furthermore, a decreasing trend of ionic conductivity is observed in the 5 wt% MnO_2 and 7 wt% MnO_2@PVA gel systems. As the viscosity of a solution increases, the ions have a harder time moving around, which decreases the ionic conductivity.[35]

CV analysis

A strong and well-liked electrochemical method is cyclic voltammetry, which is frequently used to study the reduction and oxidation processes of chemical species.[36] Fig. 3(b), (c), (d), (e) and (f) represents cyclic voltammograms of plane PVA, 1 wt% MnO_2@PVA, 3 wt% MnO_2@PVA, 5 wt% MnO_2@PVA, and 7 wt% MnO_2@PVA gel electrolytes, respectively. We recorded cyclic voltammograms at different scan rates from 10 mV s^{-1} to 100 mV s^{-1}. Sharp anodic and cathodic peaks represent the occurrence of a redox reaction. The anodic peak at −0.47 V and the cathodic peak obtained at −0.61 V represent the formation of lead sulphate from lead and lead from lead sulphate, respectively. The anodic peak at about 0 V and cathodic peak at −0.39 V indicate oxidation of a trace amount of antimony in the lead electrode and the formation of lead from lead oxide, respectively.[37] From all cyclic voltammograms, it is noted that as the scan rate increases the peak current also increases. The peak current is proportional to the rate of diffusion of the electroactive species to the electrode surface.[38] As the scan rate increases, the time available for diffusion decreases, so the current must increase to maintain the same amount of charge transfer. Fig. 3(g) displays a cyclic voltammogram of all gel systems at a fixed scan rate of 100 mV s^{-1} and Fig. 3(h) displays the variation of peak current with different wt% of MnO_2@PVA at a scan rate of 100 mV s^{-1}. Peak currents of 0.0342 A, 0.0369 A, 0.0485 A, 0.0454 A and 0.0319 A were obtained for plane PVA, 1 wt% MnO_2@PVA, 3 wt% MnO_2@PVA, 5 wt% MnO_2@PVA, and 7 wt% MnO_2@PVA gel electrolytes, respectively. From Fig. 3(g) and (h), it is observed that 3 wt% MnO_2@PVA exhibited the highest peak current among all gel systems. As the content of MnO_2 in PVA increases from 1 wt% to 3 wt% the peak current increases due to an increase in the active sites of MnO_2 in the PVA gel matrix. Further addition of MnO_2 at PVA from 5 wt% to 7 wt% causes a decrease in the peak current. This is attributed to the deformation of the gel structure or the gel's network becomes weaker. Fig. 3(i) displays the variation of peak current at different scan rates of the 3 wt% MnO_2@PVA gel system. In this case also the peak current goes on increasing as the scan rate increases. The CV results show that the 3 wt% MnO_2@PVA gel system is an optimised gel electrolyte.

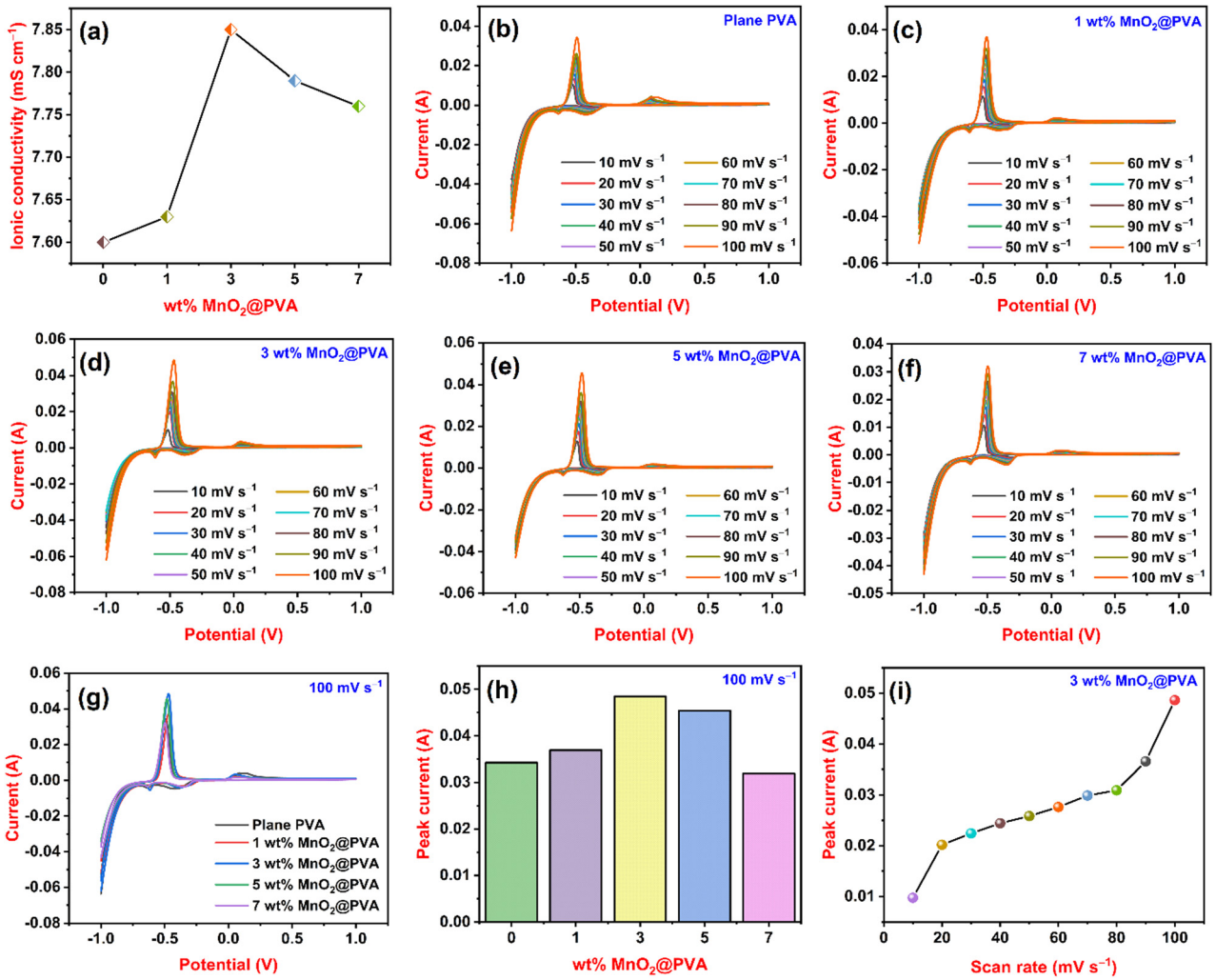

Fig. 3 (a) Variation of ionic conductivity of 0 to 7 wt% MnO_2@PVA. Cyclic voltammograms from scan rate 10 mV s^{-1} to 100 mV s^{-1} of (b) plane PVA, (c) 1 wt% MnO_2@PVA, (d) 3 wt% MnO_2@PVA, (e) 5 wt% MnO_2@PVA, and (f) 7 wt% MnO_2@PVA gel electrolytes. (g) Cyclic voltammogram of all gel electrolytes at 100 mV s^{-1}. (h) Variation of the peak current of all gel electrolytes at 100 mV s^{-1}. (i) Variation of the peak current of 3 wt% MnO_2@PVA at a scan rate from 10 mV s^{-1} to 100 mV s^{-1}.

EIS analysis

Electrochemical impedance spectroscopy is a powerful technique used to characterize the electrical properties of electrochemical systems. It is a non-destructive technique that can be used to study a wide range of systems, including batteries, fuel cells, corrosion, and biological systems.[39] Fig. 4(a) displays the Nyquist graph of plane PVA and PVA loaded with different MnO_2 along with the equivalent circuit. We used ZSimpWin 3.21 software to draw fitted curves and a selection of equivalent circuits. We used impedance parameters like R (resistance), C_{dl} (double layer capacitance), Q (constant phase element) and W (Warburg impedance) to measure the impedance nature of the formulated gel electrolyte. R_s (solution resistance) and R_{ct} (charge transfer resistance) are key findings to measure the resistance behaviour of the gel system. Table 1 represents impedance findings of all formulated gel systems. From Fig. 4(b) and Table 1, it is observed that the 3 wt% MnO_2@PVA gel system got a lower value of R_s (0.5253 Ohm) and R_{ct} (61.44 Ohm) and also a higher value of C_{dl} (0.0002015 F) and Q (0.004342 S s^n) when compared to other MnO_2 loaded PVA gels. This is attributed to the presence of more mobile ions at this concentration that can carry an electric current, which lowers the resistance and hence increases conductance.[40] The 3 wt% MnO_2@PVA gel system also shows a lower value of Warburg impedance (0.05048 S s^5). This means that it takes longer for ions to reach the electrode, which results in a lower Warburg impedance. EIS results display that the 3 wt% MnO_2@PVA gel system is the optimised gel electrolyte, which is in good agreement with the CV results.

PDP analysis

One of the most used DC electrochemical techniques in corrosion testing is the potentiodynamic polarisation measurement. Due to the large range of potentials delivered to the test electrode in PDPs, the metal surface oxidation or reduction process occurs primarily, and as a consequence, an appropriate current is produced.[41] Fig. 4(c) displays potentiodynamic polarization curves for plane

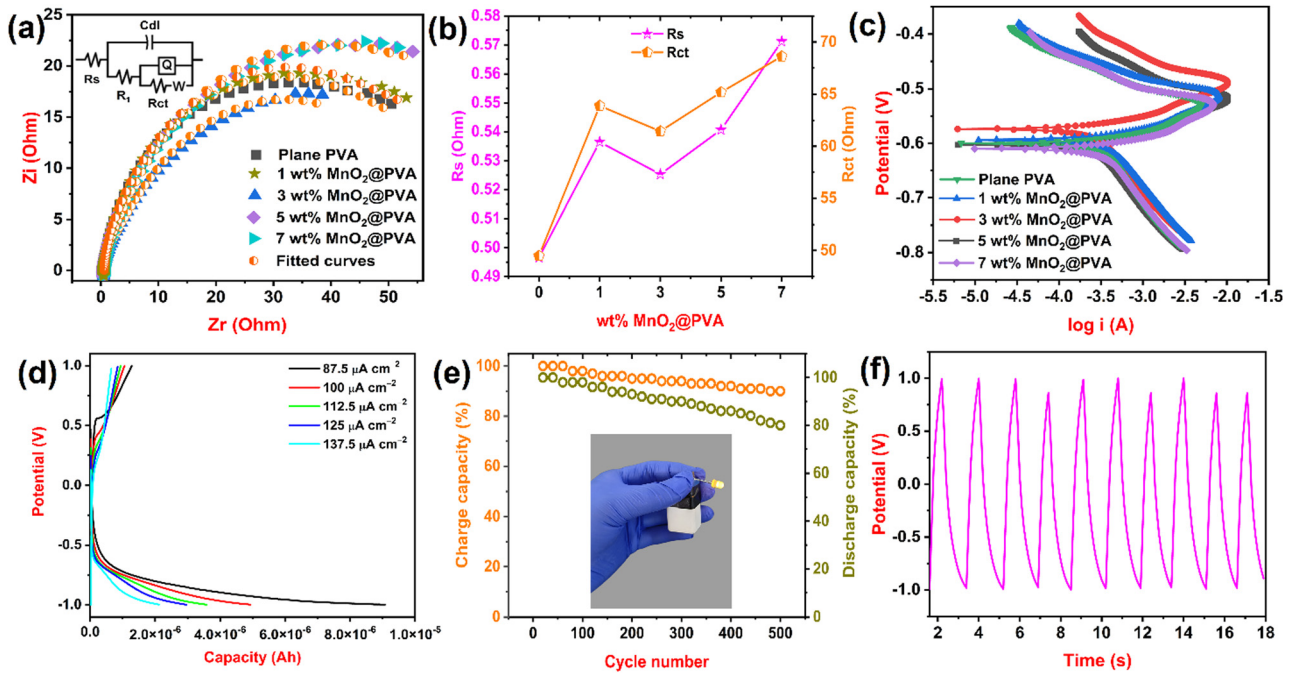

Fig. 4 (a) Nyquist plot of all gel electrolytes with an equivalent circuit. (b) Variation of the R_s and R_{ct} values. (c) Potentiodynamic polarization curves. (d) Charge and discharge capacity of the device at different current densities. (e) Cycling study of the device and photo image of the working LED using the device. (f) Charge–discharge nature of the device for the first 10 cycles.

Table 1 EIS and PDP parameters of the gel systems

Gel systems	R_s (Ohm)	C_{dl} (F)	R_1 (Ohm)	Q (S s^n)	n	R_{ct} (Ohm)	W (S s^5)	E_{corr} (V)	I_{corr} (A)
Plane PVA	0.4966	0.0001827	3.828	0.002173	0.63	49.48	0.06794	−0.6058	3.5431
1 wt% MnO_2@PVA	0.5365	0.0002001	4.696	0.002209	0.58	63.89	0.08516	−0.5901	3.5102
3 wt% MnO_2@PVA	0.5253	0.0002015	2.991	0.004342	0.62	61.44	0.05048	−0.5894	3.3641
5 wt% MnO_2@PVA	0.5407	0.0001881	6.299	0.002359	0.63	65.19	0.05583	−0.6037	3.4347
7 wt% MnO_2@PVA	0.5712	0.0001832	7.847	0.001915	0.61	68.61	0.05727	−0.6116	3.524

PVA and PVA loaded with MnO_2. Corrosion current (I_{corr}) and corrosion potential (E_{corr}) are the parameters to be analysed for gel systems. The I_{corr} and E_{corr} values of the formulated gel systems are given in Table 1. From the table, it is noted that the 3 wt% MnO_2@PVA gel system got lower I_{corr} (3.3641 A) and E_{corr} (−0.5894 V) values. A lower I_{corr} value indicates a slower rate of corrosion. This means that it is more difficult for ions to move through the gel, which slows down the corrosion reaction.[42] The PDP results help us to know that the 3 wt% MnO_2@PVA gel system is an optimised gel electrolyte that is in good agreement with the CV and EIS results.

GCD analysis

Galvanostatic charge–discharge is a method of electrochemically charging and discharging a device at a constant current. Due to its very close physical link to the capacitive charge, it has also been used to describe supercapacitors and secondary batteries.[43] We filled 3 wt% MnO_2@PVA gel electrolyte, which is optimised into a prototype battery, and performed GCD tests at various current densities. Fig. 4(d) illustrates capacity curves concerning potential. The battery showed a discharge capacity of 2.143, 2.972, 3.593, 4.948 and 9.080 μA h at current density 137.5, 125, 112.5, 100 and 87.5 μA cm^{-2}, respectively. When the current density is low, the battery has more time to electrochemically react and release its stored energy. Therefore, as the current density decreases, the discharge capacity of the battery increases.[44] The battery displayed a maximum discharge capacity of 9.080 μA h at a current density of 87.5 μA cm^{-2}. A cycling study of battery use is a test that measures the number of times a battery can be charged and discharged before it loses a significant amount of its capacity. We performed a cycling study for a battery containing optimized gel electrolyte for 500 cycles at a current density of 140 μA cm^{-2}. Fig. 4(e) shows the cycle life of the battery with respect to the percentage of charge and discharge capacity. The battery exhibited a discharge capacity of 81% after 500 prolonged cycles, which indicated remarkable cycling stability.[45] When a battery is discharged, the active materials in the electrodes undergo chemical reactions that release electrons. These reactions are reversible, but they become less efficient over time, which results in a decrease in the discharge capacity.[46] Fig. 4(e) also shows the photo-image of the battery used to light the LED. The nature of the charge–discharge curves during the

cycling study is displayed in Fig. 4(f). Thus, we used 3 wt% MnO_2@PVA gel electrolyte in the battery and showed its working using the GCD technique.

Conclusions

In this research work, we formulated gel systems of PVA matrix loaded with various amounts of MnO_2 for the VRLA battery. The marginal decrease in the expansion of the characteristic peaks in FTIR suggested the influence of MnO_2 in the PVA gel matrix. From the ionic conductivity study, it is noted that 3 wt% MnO_2@PVA gel electrolyte showed a maximum ionic conductance of 7.85 mS cm^{-1}. In CV analyses, the highest anodic peak current of 0.0369 A is observed for the 3 wt% MnO_2@PVA gel electrolyte. EIS techniques suggested that the 3 wt% MnO_2@PVA gel electrolyte is the optimized gel system due to its lower R_s (0.5253 Ohm) and R_{ct} (61.44 Ohm) values. Findings of the PDP technique witnessed that the 3 wt% MnO_2@PVA gel electrolyte has the lowest I_{corr} value of 3.364 A. Furthermore, the GCD technique of the prototype battery comprising 3 wt% MnO_2@PVA gel electrolyte exhibited the highest discharge capacity of 9.080 μA h at a current density of 87.5 μA cm^{-2}. After 500 cycles, the battery displayed 81% discharge capacity. All these electrochemical findings suggested that MnO_2 can boost the performance of VRLA batteries.

Author contributions

Bipin S. Chikkatti: conceptualization, methodology, writing – original draft. Ashok M. Sajjan: resources, conceptualization, writing – review & editing, formal analysis, investigation, supervision. Nagaraj R. Banapurmath: project administration, writing – review & editing.

Conflicts of interest

There are no conflicts to declare.

Acknowledgements

One of the authors (Ashok M. Sajjan) acknowledges financial support from VGST, Karnataka, India (No. K-FIST(L2)/2016-17/GRD-540/2017-18/103/310).

References

1 P. T. Moseley, Characteristics of a high-performance lead/acid battery for electric vehicles-an ALABC view, *J. Power Sources*, 1997, **67**, 115–119.
2 V. Svoboda, H. Doering and J. Garche, *J. Power Sources*, 2005, **144**, 244–254.
3 P. T. Moseley, *J. Power Sources*, 2004, **127**, 27–32.
4 M. L. Soria, J. Valenciano, A. Ojeda, G. Raybaut, K. Ihmels, J. Deiters, N. Clement, J. Morales and L. Sánchez, *J. Power Sources*, 2003, **116**, 61–72.
5 X. Sun and J. Zhao, *Electrochemistry*, 2016, **84**, 578–584.
6 M. G. Insinga, A. Derelitto, S. Pisana, R. L. Oliveri, C. Sunseri and R. Inguanta, *Chem. Eng. Trans.*, 2019, **73**, 25–30.
7 E. Aram, M. Ehsani and H. A. Khonakdar, *Thermochim. Acta*, 2015, **615**, 61–67.
8 J. Duan, Q. Tang, R. Li, B. He, L. Yu and P. Yang, *J. Power Sources*, 2015, **284**, 369–376.
9 X. Wang and H. G. Spencer, Calcium alginate gels: formation and stability in the presence of an inert electrolyte, *Polymer*, 1998, **39**(13), 2759–2764.
10 L. P. Teo, M. H. Buraidah and A. K. Arof, *Ionics*, 2020, **26**, 4215–4238.
11 Y. Zhang, D. Cheng, Z. Wu, F. Li, F. Fang and Z. Zhan, *Chemosensors*, 2020, **8**, 1–14.
12 M. Wang, J. Bai, K. Shao, W. Tang, X. Zhao, D. Lin, S. Huang, C. Chen, Z. Ding and J. Ye, *Int. J. Polym. Sci.*, 2021, **2021**, 1–16.
13 E. Otsuka, S. Komiya, S. Sasaki, J. Xing, Y. Bando, Y. Hirashima, M. Sugiyama and A. Suzuki, *Soft Matter*, 2012, **8**, 8129–8136.
14 B. Karaman and A. Bozkurt, *Int. J. Hydrogen Energy*, 2018, **43**, 6229–6237.
15 C. Wang, K. Hu, Y. Liu, M. R. Zhang, Z. Wang and Z. Li, *Materials*, 2021, **14**, 1955.
16 J. Wang, H. Chi, A. Zhou, R. Zheng, H. Bai and T. Zhang, *RSC Adv.*, 2020, **10**, 22019–22026.
17 S. A. Ansari, M. M. Khan, S. Kalathil, A. Nisar, J. Lee and M. H. Cho, *Nanoscale*, 2013, **5**, 9238–9246.
18 Y. Zhang, S. Deng, M. Luo, G. Pan, Y. Zeng, X. Lu, C. Ai, Q. Liu, Q. Xiong, X. Wang, X. Xia and J. Tu, *Small*, 2019, **15**, 1905452.
19 V. G. Bhide and R. H. Dani, *Physica*, 1961, **27**, 821–826.
20 C.-C. Yang and S.-J. Lin, Improvement of high-rate capability of alkaline Zn ± MnO_2 battery, *J. Power Sources*, 2002, **112**, 174–183.
21 J. Chen, W. De Zhang and J. S. Ye, *Electrochem. Commun.*, 2008, **10**, 1268–1271.
22 M. Zhang, Y. Chen, D. Yang and J. Li, *J. Energy Storage*, 2020, **29**, 101363.
23 N. Zhang, L. Li, Y. Guo, J. He, R. Wu, L. Song, G. Zhang, J. Zhao, D. Wang and H. He, *Appl. Catal., B*, 2020, **270**, 118860.
24 Q. Li, Z. L. Wang, G. R. Li, R. Guo, L. X. Ding and Y. X. Tong, *Nano Lett.*, 2012, **12**, 3803–3807.
25 K. M. Racik, K. Guruprasad, M. Mahendiran, J. Madhavan, T. Maiyalagan and M. V. A. Raj, *J. Mater. Sci.: Mater. Electron.*, 2019, **30**, 5222–5232.
26 M. Huang, Y. Zhang, F. Li, L. Zhang, R. S. Ruoff, Z. Wen and Q. Liu, *Sci. Rep.*, 2014, **4**, 3878.
27 S. A. Moon, B. K. Salunke, B. Alkotaini, E. Sathiyamoorthi and B. S. Kim, *IET Nanobiotechnol.*, 2015, **9**, 220–225.
28 S. Mallakpour and F. Motirasoul, *Prog. Org. Coat.*, 2017, **103**, 135–142.
29 M. A. Abureesh, A. A. Oladipo and M. Gazi, *Int. J. Biol. Macromol.*, 2016, **90**, 75–80.
30 Y. Khairy, I. S. Yahia and H. Elhosiny Ali, *J. Mater. Sci.: Mater. Electron.*, 2020, **31**, 8072–8085.
31 B. S. Chikkatti, A. M. Sajjan, P. B. Kalahal, N. R. Banapurmath, T. M. Y. Khan, S. D. A. Khadar, S. M. Shamsudeen and A. B. Raju, *Gels*, 2022, **8**, 791.
32 B. S. Chikkatti, A. M. Sajjan, P. B. Kalahal and N. R. Banapurmath, *J. Energy Storage*, 2023, **72**, 108261.

33 J. Owen, Introduction 669 21.2 the conduction mechanism 671 21.2.1 Ionic Mobility in Solids 671 21.2.2 Ionic Mobility in Liquids 673.
34 J. Experton, X. Wu, G. Wang and C. R. Martin, *ChemElectroChem*, 2018, **5**, 3113–3120.
35 H. Yoon, A. S. Best, M. Forsyth, D. R. MacFarlane and P. C. Howlett, *Phys. Chem. Chem. Phys.*, 2015, **17**, 4656–4663.
36 N. Elgrishi, K. J. Rountree, B. D. McCarthy, E. S. Rountree, T. T. Eisenhart and J. L. Dempsey, *J. Chem. Educ.*, 2018, **95**, 197–206.
37 B. S. Chikkatti, A. M. Sajjan, P. B. Kalahal and N. R. Banapurmath, *J. Energy Storage*, 2023, **72**, 108261.
38 B. S. Chikkatti, A. M. Sajjan, P. B. Kalahal, N. R. Banapurmath and N. H. Ayachit, *J. Energy Storage*, 2023, **72**, 108513.
39 N. Meddings, M. Heinrich, F. Overney, J. S. Lee, V. Ruiz, E. Napolitano, S. Seitz, G. Hinds, R. Raccichini, M. Gaberšček and J. Park, *J. Power Sources*, 2020, 480.
40 K. H. Teoh, C. S. Lim and S. Ramesh, *Measurement*, 2014, **48**, 87–95.
41 J. Telegdi, A. Shaban and G. Vastag, *Encyclopedia of Interfacial Chemistry: Surface Science and Electrochemistry*, Elsevier, 2018, pp. 28–42.
42 N. C. Rosero-Navarro, L. Paussa, F. Andreatta, Y. Castro, A. Durán, M. Aparicio and L. Fedrizzi, *Prog. Org. Coat.*, 2010, **69**, 167–174.
43 C. Yun and S. Hwang, *ACS Omega*, 2021, **6**, 367–373.
44 X. Guo, C. Wang, W. Wang, Q. Zhou, W. Xu, P. Zhang, S. Wei, Y. Cao, K. Zhu, Z. Liu, X. Yang, Y. Wang, X. Wu, L. Song, S. Chen and X. Liu, *Nano Res. Energy*, 2022, **1**, e9120026.
45 H. Ge, X. Feng, D. Liu and Y. Zhang, *Nano Res. Energy*, 2023, **2**, e9120039.
46 L. Mai, X. Tian, X. Xu, L. Chang and L. Xu, *Chem. Rev.*, 2014, **114**, 11828–11862.